ENHANCING FLOW STRUCTURE IN HEAT EXCHANGERS Analysis of Dynamic and Thermal Air-Flow Behavior with Perforated and Inclined Baffles

by

Sultan ALQAHTANI[a], Sultan ALSHEHERY[a], Mustafa BAYRAM[b*], Omolayo M. IKUMAPAYI[c,d], Esther T. AKINLABI[e], Stephen A. AKINLABI[e], and Younes MENNI[f,g]

[a] College of Engineering, Mechanical Engineering Department, King Khalid University, Abha, Saudi Arabia
[b] Department of Computer Engineering, Biruni University, Istanbul, Turkey
[c] Department of Mechanical and Mechatronics Engineering, Afe Babalola University, Ado Ekiti, Nigeria
[d] Department of Mechanical Engineering Science, University of Johannesburg, South Africa
[e] Department of Mechanical and Construction Engineering, Faculty of Engineering and Environment, Northumbria University, Newcastle, UK
[f] Department of Technology, University Center Salhi Ahmed Naama (Ctr. Univ. Naama), Naama, Algeria
[g] College of Engineering, National University of Science and Technology, Dhi Qar, Iraq

Original scientific paper
https://doi.org/10.2298/TSCI2304269A

This paper presents a comprehensive analysis of the dynamic and thermal behavior of air-flow within a heat exchanger equipped with two distinctive baffles: a perforated baffle and a partially inclined baffle. The influence of hole positioning in the perforated baffle on the overall performance of the heat exchanger is thoroughly investigated through a systematic examination of temperature curves at varying Reynolds number values. The results demonstrate significant enhancements in flow characteristics attributed to the presence of these baffles. The flow structure exhibits prominent main currents across the gaps and secondary currents through the holes. The inclusion of these barriers leads to significant deformations and the emergence of well-developed recycling cells in the form of vortices. Both the perforated and inclined baffles effectively reduce pressure values on their frontal regions, thereby mitigating friction losses. Furthermore, the introduction of a perforation in the lower part of the baffle induces a more turbulent flow compared to the other cases. This is attributed to the expansion of the recirculating cells, resulting in improved fluid mixing and subsequent enhancement of thermal energy gain. These findings offer valuable insights into the design and optimization of heat exchangers, enabling improved performance and efficiency in various engineering applications.

Key words: *CFD, SIMPLE, QUICK, Reynolds number, vortex, fluid mixing*

Introduction

Channel heat exchangers (HE) are a vital component in the industrial field, playing a crucial role in efficient heat transfer (HT) processes [1]. These HE come in various types, each designed to suit specific applications and requirements. Plate-and-frame HE consist of a

* Corresponding author, e-mail: mbayram34@gmail.com

series of plates with corrugated patterns, allowing for increased surface area and enhanced HT efficiency [2]. Shell-and-tube HE utilize a shell filled with tubes, enabling the exchange of heat between two fluids [3]. Another type is the finned-tube HE, where finned surfaces enhance HT effectiveness by expanding the heat transfer area [4]. Channel HE facilitate the transfer of thermal energy from one medium to another, enabling effective cooling, heating, or temperature regulation in industrial processes. By efficiently transferring heat, these HE enhance productivity, reduce energy consumption, and optimize overall system performance, making them indispensable in various industrial sectors [5].

Using HE channels is of paramount importance in many industries due to their significant benefits [6]. Firstly, HE channels allow for efficient heat transfer between fluids, enabling precise control of temperatures in industrial processes [7]. This capability ensures optimal performance and productivity while maintaining the integrity of equipment and materials. Secondly, HE channels facilitate energy conservation by harnessing waste heat and redirecting it for other applications, reducing overall energy consumption and promoting sustainability [8]. Additionally, the use of channels in HE enhances system reliability by preventing cross-contamination between fluids, ensuring the purity and integrity of each medium. This is especially critical in sectors such as food and pharmaceutical industries, where maintaining product quality is essential [9]. Overall, employing HE channels improves process efficiency, minimizes energy waste, and upholds product integrity, making them indispensable tools in numerous industrial applications [10].

Numerous strategies exist for enhancing the performance and efficiency of HE channels [11]. One approach is to enhance the design of the channels by incorporating advanced geometries. For instance, employing fins or turbulators on the channel walls increases the surface area available for HT, thereby improving overall heat exchange efficiency [12]. Another method involves optimizing the fluid-flow characteristics within the channels. By adjusting the flow rate, ensuring uniform distribution, and reducing pressure losses, the HT process can be significantly enhanced. Additionally, using high-performance materials with excellent thermal conductivity can improve the overall HT rate [13]. Proper maintenance and cleaning of HE channels are also crucial to prevent fouling and scaling, which can hinder HT efficiency. Lastly, incorporating advanced monitoring and control systems can aid in real-time performance evaluation and adjustment, ensuring the HE channels operate at their optimal levels. By implementing these strategies, the performance of HE channels can be maximized [14], resulting in improved HT efficiency and enhanced industrial processes [15].

Passive techniques have a pivotal role in increasing the performance of HE channels, offering several advantages in terms of efficiency and simplicity [16]. One key advantage is that passive methods do not require additional energy input or complex mechanical systems, making them cost-effective and easy to implement. For instance, incorporating proper channel geometry and optimizing the flow path can promote natural convection and induce turbulence, enhancing HT without the need for external forces. Passive methods also include the use of surface enhancements such as extended surfaces [17] or microstructures, which increase the effective surface area and promote better HT. These techniques encourage improved fluid mixing, reduced thermal boundary layers, and enhanced convective HT, leading to more efficient operation of the HE channels [18]. Moreover, passive methods often contribute to increased reliability and reduced maintenance requirements, as they minimize the risk of mechanical failures and reduce the likelihood of fouling or scaling [19]. Overall, the importance of passive methods in increasing HE channel performance lies in their ability to enhance efficiency, reduce costs, and simplify operation and maintenance procedures [20].

The primary objective of this analysis is to extensively investigate and delve into the utilization of partially slanted and perforated single-hole baffles within HE channels, specifically examining the influence of hole positioning on the overall efficiency of the HE. This study aims to delve into the potential of these innovative baffle designs to significantly enhance HT transfer performance, by manipulating the flow characteristics and optimizing the surface area for heat exchange. By incorporating partially oblique baffles, which are inclined at an angle to the flow direction (α = 45°), and perforated single-hole baffles, which introduce localized fluid interaction, the researchers aim to determine the impact of these design modifications on hydrothermal behavior. Additionally, the study aims to assess the influence of hole station in the perforated single-hole baffles, examining how different hole positions influence flow rates and overall exchanger performance. The findings of this study will contribute significantly to the optimization of HE channels, providing valuable insights for enhancing the efficiency and effectiveness of HT systems in various industrial applications.

Modeling of the studied HE channel

The investigated HE channel is a rectangular channel with a narrow entrance and a wide exit, as depicted in fig. 1. The channel incorporates two baffles of distinct models. The initial configuration entails a single-hole baffle securely positioned on the upper segment of the channel. Conversely, the alternative setup incorporates a baffle attached to the lower wall, featuring an inclined upper section angled at 45° towards the channel exit. The design of the examined channel model draws inspiration from previous studies conducted by Demartini *et al.* [21] and Mahdi *et al.* [22], with all dimensions comprehensively illustrated in the accompanying figure.

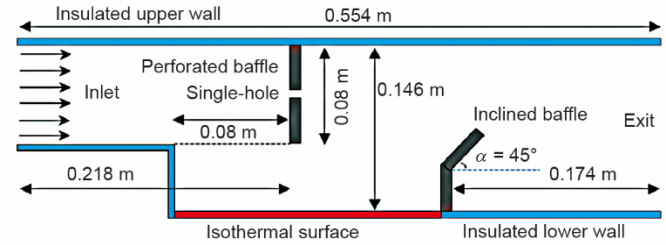

Figure 1. Representation of the HE channel under investigation

This study aims to analyze the impact of the perforated baffle by varying the position of the perforation across the entire surface of this same vortex generator, according to four possible cases, as shown in fig. 2. By exploring this effect, the researchers seek to gain insights into the performance enhancement potential of the perforated baffle design in the HE channel.

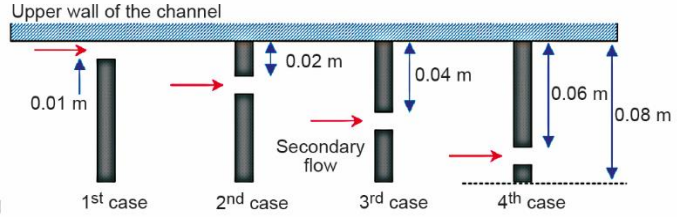

Figure 2. Illustration of the perforated baffle models employed in the study

Several simplifications were employed in the study to facilitate this CFD simulation. Firstly, the fluid (air) utilized in the current situation is assumed to be Newtonian, implying that its flow behavior follows classical fluid mechanics principles. Additionally, the fluid is considered incompressible, neglecting any changes in density due to pressure variations. Another simplification involves assuming a uniform velocity profile at the inlet of the exchanger, simplifying the initial flow conditions for analysis. The lower part of the channel, where heat is transferred, is assumed to have a constant temperature of 100 °C, simplifying the heat boundary conditions. Moreover, the channel walls are set with non-slip and impermeable constraints, assuming that there is no relative motion between the fluid and the walls, and no fluid can penetrate through the walls. Finally, the outlet of the channel is assigned the atmospheric pressure as the specified condition, simplifying the analysis of fluid behavior as it approaches the exit.

These simplifications aid in focusing on specific aspects of the heat exchanger channel while providing a basis for initial analysis and insights into the system's behavior. The modeling of steady turbulent flow involves the utilization of three equations [23]:
The continuity:

$$\nabla\vec{\mathrm{V}} = 0 \tag{1}$$

The momentum:

$$\rho(\vec{\mathrm{V}}\nabla\vec{\mathrm{V}}) = -\nabla P + \mu_{\mathrm{f}}\nabla^2\vec{\mathrm{V}} \tag{2}$$

and the energy:

$$\rho C_P(\vec{\mathrm{V}}\nabla T) = k_{\mathrm{f}}\nabla^2 T \tag{3}$$

To accurately represent the turbulent phenomenon present in the channel, the modeling process incorporates the utilization of the standard k-ε model. This approach is founded on the premise that turbulent flows are predominantly influenced by the kinetic energy, K, and the rate, ε, of dissipation, as they are considered the key variables in such scenarios. The model solves transport equations for k and ε, taking into account the effects of turbulence production, diffusion, and dissipation. By implementing the standard k-ε model, the turbulent flow characteristics, such as turbulence intensity and eddy viscosity, can be predicted, providing valuable insights into the behavior of turbulent flows within the channel.

The equation governing turbulent kinetic energy [24]:

$$\frac{\partial}{\partial x_j}(\rho \mathrm{Ku}_j) = \frac{\partial}{\partial x_j}\left[\left(\mu + \frac{\mu_t}{\sigma_K}\right)\frac{\partial K}{\partial x_j}\right] + G_K - \rho\varepsilon \tag{4}$$

and the equation describing the rate, ε, within the model is:

$$\frac{\partial}{\partial x_j}(\rho\varepsilon u_j) = \frac{\partial}{\partial x_j}\left[\left(\mu + \frac{\mu_t}{\sigma_\varepsilon}\right)\frac{\partial \varepsilon}{\partial x_j}\right] + C_{1\varepsilon}\frac{\varepsilon}{K}G_K - C_{2\varepsilon}\rho\frac{\varepsilon^2}{K} \tag{5}$$

where ρ is the density of the fluid, $\vec{\mathrm{V}}$ – the vector of velocity, P – the pressure of the fluid, μ – the fluid dynamic viscosity, k – the fluid thermal conductivity, and $C_{1\varepsilon}$, $C_{2\varepsilon}$, σ_K, and σ_ε represent the turbulence model constants, as determined by Launder and Spalding [24]. The parameter known as the Reynolds number can be described as a dimensionless quantity and can be defined in the subsequent manner:

$$\mathrm{Re} = \frac{\rho u_{\mathrm{in}} D_{\mathrm{h}}}{\mu} \tag{6}$$

where u_{in} is the inlet velocity and D_{h} – the hydraulic diameter of the channel.

The governing equations are effectively solved using the finite volume method, along with the highly regarded SIMPLE algorithm and QUICK scheme [25, 26]. These computational techniques are implemented within the widely used CFD software, ANSYS FLUENT.

To ensure accurate representation of the physical domain, structured meshes consisting of rectangular cells were employed. Special attention was given to refine the mesh along solid boundaries, capturing boundary layer phenomena and accurately representing flow dynamics. In regions further from the walls, a uniform mesh was utilized to strike a balance between computational efficiency and accuracy [21]. In the present study, a comprehensive comparison was conducted to analyze the *x*-velocity values under various cases, specifically focusing on the exit region and a constant Reynolds number value of $8.73 \cdot 10^4$, while considering different hydraulic diameters, fig. 3. The comparison involved juxtaposing the findings of the current study with the experimental and numerical data from Demartini *et al.* [21].

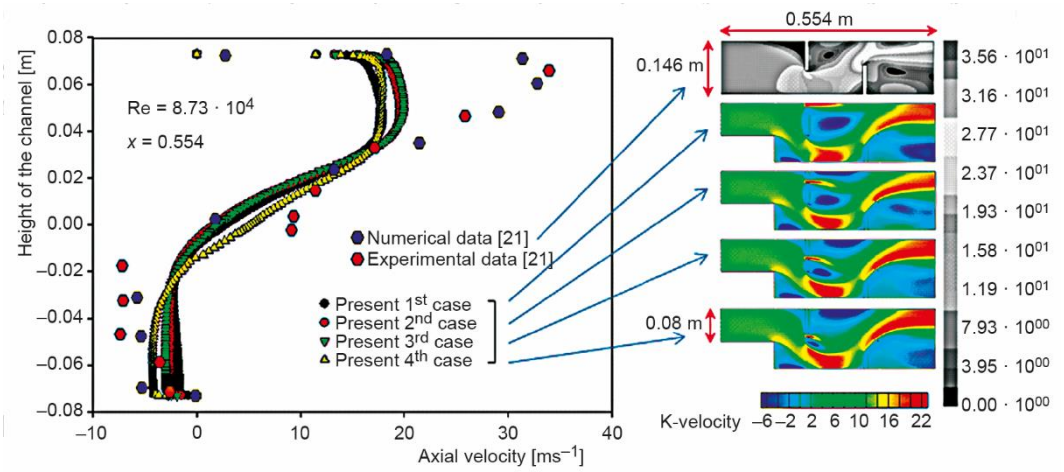

Figure 3. Comprehensive comparison between the numerical and experimental axial velocity values, focusing on a fixed Reynolds number and various hydraulic diameters

The results revealed a proportional behavior in terms of the flow characteristics, indicating similarities between the two sets of data. However, notable differences in the velocity values emerged, primarily attributed to variations in the entrance height and distinct baffle designs employed in the present experiments. Importantly, this comparison effectively demonstrated the convergence of the two behaviors and highlighted the impact of utilizing new models, as reflected in the distinct velocity values obtained. These findings emphasize the significance of considering entrance conditions and design variables in accurately predicting and understanding fluid-flow phenomena.

Results and discussions

The following section presents the results and discussions obtained from the conducted study. The obtained data and analysis shed light on various aspects related to the in-

vestigated phenomenon, providing insights into key findings, trends, and significant observations. These results will be thoroughly examined and discussed, aiming to deepen our understanding and contribute to the existing body of knowledge in the field.

Figure 4 presents the observed changes in air-flow patterns within the channel, illustrating the effect of baffles on the flow structure across various tested scenarios. From the left side of the initial baffle to the channel outlet, the influence of baffles becomes evident. The first baffle deflects the flow downward, leading to the formation of vortices on the left side of the heated space and behind the same baffle. Moreover, the presence of a hole induces the emergence of a secondary current, traversing the vortex cells situated behind this initial baffle. The second baffle redirects the air field towards the top HE section, facilitating the formation of a large recirculation zone behind it. Overall, the presence of baffles introduces a distinct flow structure characterized by notable rotating cells. Upon comparing the various cases, it is evident that the inclusion of a hole at the bottom of the baffle (Case 4, fig. 2) induces a strong structure with significant recirculation cells. This configuration fosters efficient fluid mixing compared to the other cases.

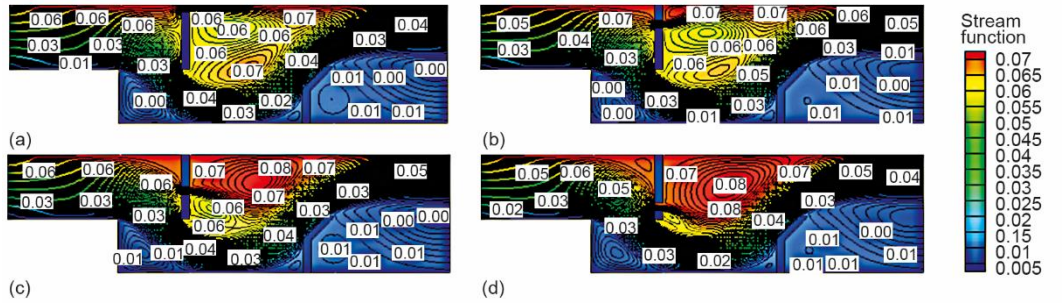

Figure 4. Streamline variations for Re = 5000 across diverse investigated scenarios; (a) initial baffle in 1st instance, (b) initial baffle in 2nd instance, (c) initial baffle in 3rd instance, and (d) initial baffle in 4th instance

Upon conducting a comprehensive analysis of the dynamic *P* fields, as depicted in fig. 5, it becomes apparent that the primary flow demonstrates a sinusoidal motion, propagating from the left side to the right while experiencing notable wall friction. Within the main stream, distinct *P* enhancements are concentrated in multiple areas, such as the narrow spaces and the perforated baffle gaps. Moreover, the highest *P* values align precisely with the leading edges of the two obstructions. Conversely, a significant pressure reduction is observed in numerous regions, particularly those located downstream of the obstacles, leading to the emergence of vortices with diverse magnitudes.

The field examination further uncovers that various configurations of obstructions produce unique impacts on pressure distribution. For instance, the inclusion of an aperture assists in alleviating pressure, particularly in the frontal section of the upper obstruction. On the other hand, the second obstacle effectively reduces pressure through an inclined technique implemented on its upper part. Moreover, the positioning of the hole also influences the pressure dynamics, as evident in the remarkable pressure rise when the hole is located in the lower part of the baffle (Case 4, fig. 2). This particular configuration facilitates the formation of high intensity recirculation cells, leading to effective fluid mixing with the hot spaces.

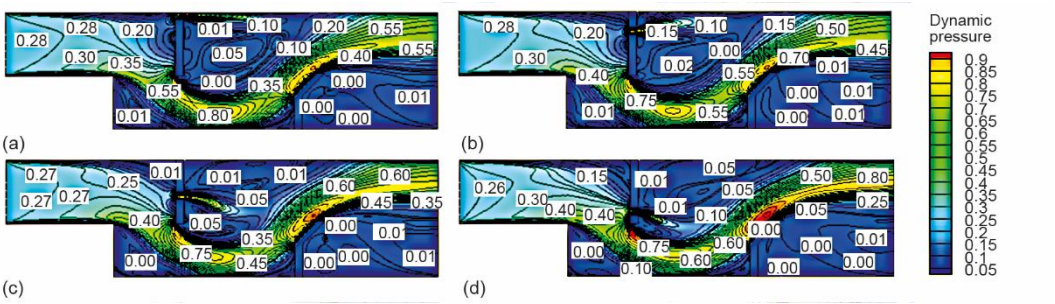

Figure 5. Dynamic pressure fields across multiple Re = 5000 cases, illustrating the varied flow behaviors; (a) initial baffle in 1st instance, (b) initial baffle in 2nd instance, (c) initial baffle in 3rd instance, and (d) initial baffle in 4th instance

Figure 6 depicts the average velocity variations across different scenarios, maintaining a consistent Reynolds number value of $5 \cdot 10^3$. Velocity values are lower in all areas containing the recirculating cells, behind the baffles, and on the left side of the hot space. However, the speed values noticeably improve across the gaps, below the perforated baffle, and above the inclined baffle. The presence of the hole also allowed the formation of a secondary current with high speeds, further influencing the flow patterns. Moreover, the presence of a second baffle with a slanted upper part allowed the fluid to flow gently towards the outlet, enhancing the overall fluid dynamics. Interestingly, among the tested cases, the fourth case exhibited the highest rate of velocity, indicating a structure with high mixing intensity and improved flow characteristics.

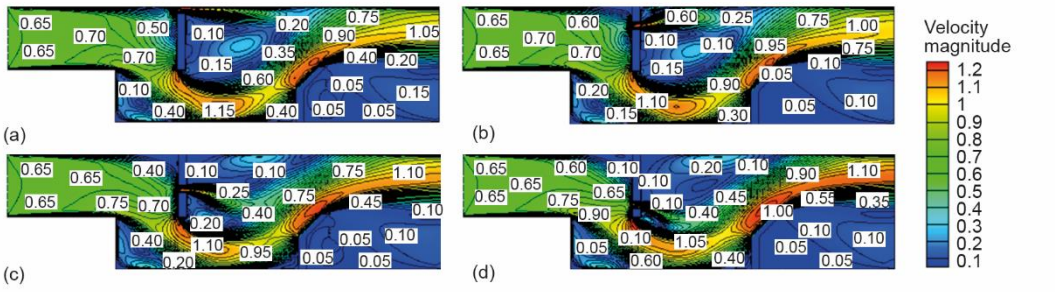

Figure 6. Unveiling the diverse average velocity fields in the studied cases at Re = 5000; (a) initial baffle in 1st instance, (b) initial baffle in 2nd instance, (c) initial baffle in 3rd instance, and (d) initial baffle in 4th instance

The axial velocity, which represents the velocity in the horizontal direction, exhibited a wide range of values across its scale, fig. 7. Both positive and negative values were observed, reflecting the flow characteristics in different regions. Negative values indicated the presence of fluid recirculation or opposing currents near the right sides of the walls. These vortices manifested as a consequence of the main current separating at the edges of these obstacles. An intriguing observation was made with the presence of a perforated baffle pore, which introduced a notable influence by dividing the flow patterns after the top vortex generator.

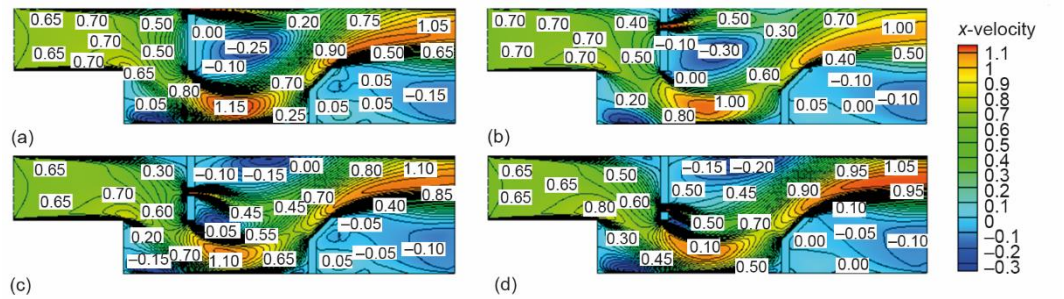

Figure 7. Contours of axial velocity in diverse cases (Re = 5000); (a) initial baffle in 1st instance, (b) initial baffle in 2nd instance, (c) initial baffle in 3rd instance, and (d) initial baffle in 4th instance

Additionally, the primary flow exhibited a slight elevation as it traversed the initial gap positioned at the front of the perforated turbulator. A progressive augmentation in velocity was observed through the subsequent gap situated beneath the same turbulator. Notably, a rapid acceleration of the main flow occurred through the third gap positioned above the 2nd turbulator, just beyond the left edge of its upper surface. Both the perforated and oblique configurations contributed to improving the air dynamics, specifically in relation to the lower perforation (case 4). These findings highlight the influence of different configurations on the flow dynamics and suggest potential improvements for optimizing fluid behavior in similar systems.

The transversal velocity scale reveals distinct patterns with a mix of negative and positive values, fig. 8. As expected, positive values represent currents flowing towards the top regions of the HE. Notably, the flow adjacent to the frontal areas of the second obstruction exhibits positive values. Moreover, the highest transverse velocity values are mainly concentrated on the inclined section. Conversely, the flow passing through the initial turbulator exhibits negative transverse velocity values, specifically on the front head of the perforated barrier. This can be attributed to the downward acceleration of the flow, contrary to the OY-axis direction. While the structure of the transversal velocity remains consistent across all cases, the intensity varies significantly. These observations highlight the complex interplay between vertical flow dynamics and the unique characteristics of the obstacles, providing valuable insights into the behavior of the system.

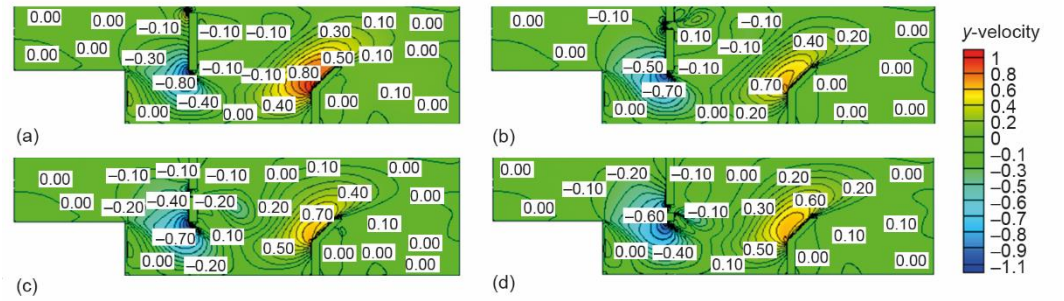

Figure 8. Contours of transversal velocity in diverse cases (Re = 5000); (a) initial baffle in 1st instance, (b) initial baffle in 2nd instance, (c) initial baffle in 3rd instance, and (d) initial baffle in 4th instance

Figure 9 provides a detailed examination of the axial velocity profiles occurring between the initial and subsequent obstructions, specifically at the axial position of x = 0.3 m. By focusing on this specific region, a deeper understanding of the fluid-flow dynamics and the influence of the obstacles on the velocity distribution is revealed. The profiles offer valuable insights into the variations and patterns of axial velocity, shedding light on the complex interactions between the obstacles and the flowing fluid. The observation of negative velocities in this particular area signifies the presence of a significant recirculation cell. Interestingly, the incorporation of a hole in the system facilitated the release of a portion of this vortex, resulting in altered flow behavior.

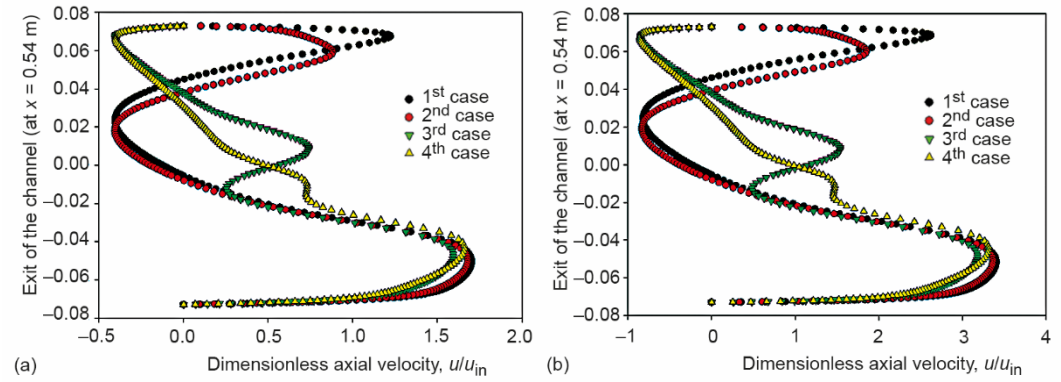

Figure 9. Analysis of velocity distribution along the axial direction between initial and subsequent obstructions at x = 0.3 m; (a) at Re = $5 \cdot 10^3$ and (b) at Re = $10 \cdot 10^3$

This phenomenon primarily manifests in higher section of the flow area. In contrast, in the lower region, the current exhibits high velocities adjacent to the inclined area, guiding the flow towards the outlet. Notably, the first bottom-hole baffle (Case 4) contributes to an enlargement of the vortex situated behind it, thereby promoting enhancements in the overall flow structure. As the Reynolds number increases, the flow intensity amplifies, primarily due to the enlargement of recirculating cells. This phenomenon can be attributed to the greater inertia and momentum of the fluid as the Reynolds number rises. The higher flow tension results in more vigorous and pronounced recirculation patterns within the system. The increased size of the recirculating cells indicates a more energetic and dynamic flow behavior, emphasizing the notable impact of Reynolds number on the strength and properties of the fluid-flow.

The examined structure demonstrates distinct limit conditions that impact the thermal behavior of the lower HE portions, encompassing the area from the left boundary to the frontal region of the second barrier. In this region, a constant temperature of 100 °C is maintained. The thermal field, denoted by T, is significantly impacted by the presence of inclined and perforated baffles. Notably, temperature increases are observed at two distinct corners: One corner can be found at the rear of the HE left side, while the other is situated in front of the left surface of the bottom turbulator. These corners serve as focal points for the formation of small vortices induced by pressure drops in their respective areas. The figure vividly illustrates these phenomena, highlighting the temperature variations and the associated flow patterns within the channel, fig. 10.

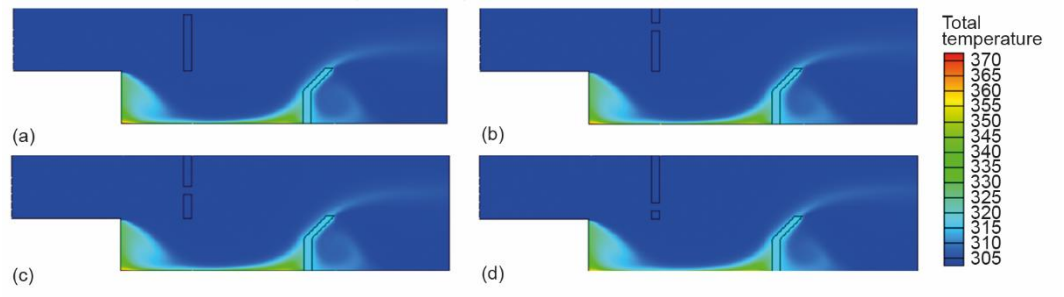

Figure 10. Contours of total temperature in diverse cases (Re = 5000); (a) initial baffle in 1st instance, (b) initial baffle in 2nd instance, (c) initial baffle in 3rd instance, and (d) initial baffle in 4th instance

Notably, the alignment of the initial obstacle effectively facilitates high-speed air-flow towards the heated region, resulting in a temperature reduction within the region exhibiting a significant temperature gradient. These observations provide valuable insights into the thermal dynamics within the system and emphasize the impact of the baffles on temperature distribution and gradients.

Moreover, it is clear that flow rates and fluid temperature within the HE exhibit a mutually influential relationship. These findings offer valuable insights into the thermal dynamics and heat transfer characteristics of the system, as illustrated in fig. 11.

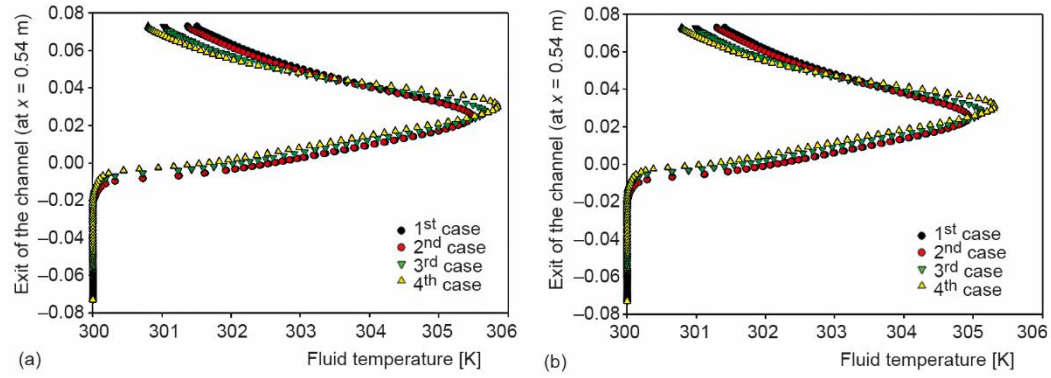

Figure 11. Exploring fluid temperature profiles at the channel exit; (a) at Re = $5 \cdot 10^3$ and (b) at Re = $10 \cdot 10^3$

This temperature increase can be attributed to the effective mixing of the fluid with the hot spaces, facilitated by the expansion of the recirculation cell areas. The perforations in the baffles played a crucial role in enhancing the fluid dynamics, allowing for improved mixing and heat transfer. As a result, the temperature at the outlet experienced a significant increase, highlighting the effectiveness of this configuration in promoting efficient heat exchange within the system.

Conclusions

The key findings can be summarized as follows.

- Comprehensive analysis of dynamic and thermal behavior of air-flow in a heat exchanger with two distinctive baffles: perforated and partially inclined.

- Thorough investigation of hole positioning in the perforated baffle and its impact on overall heat exchanger performance.
- Significant enhancements in flow characteristics observed with the presence of baffles.
- Flow structure exhibits prominent main currents across gaps and secondary currents through holes.
- Baffles induce desirable pressure drop and facilitate formation of well-developed recirculating cells (vortices).
- Both perforated and inclined baffles effectively reduce pressure values on frontal regions, minimizing friction losses.
- Introduction of perforation in lower part of baffle (Case 4) promotes more turbulent flow, expanding recirculating cells and enhancing fluid mixing.
- Valuable insights for heat exchanger design and optimization, leading to improved performance and efficiency in diverse engineering applications.

Here are some suggestions for future studies related to the analysis of air-flow in heat exchangers:

- Investigation of different baffle designs: explore the effects of various baffle geometries, such as different hole arrangements, shapes, and orientations, to further optimize flow characteristics and heat transfer performance.
- Multi-objective optimization: perform optimization studies considering multiple objectives, such as maximizing heat transfer efficiency while minimizing pressure drop or optimizing the heat exchanger design for specific applications.

Acknowledgment

The authors extend their appreciation to the Deanship of Scientific Research at King Khalid University for funding this work through large group Research Project under grant number RGP2/290/44.

References

[1] Rebhi, R., *et al.*, Forced-Convection Heat Transfer in Solar Collectors and Heat Exchangers: A Review, *Journal of Advanced Research in Applied Sciences and Engineering Technology*, *26* (2022), 3, pp. 1-15
[2] Singh, S., *et al.*, A Detailed Insight Into the Optimization of Plate and frame Heat Exchanger Design by Comparing Old and New Generation Metaheuristics Algorithms, *Journal of the Indian Chemical Society*, *99* (2022), 2, 100313
[3] Kucuk, H., The Effect of Minichannels on the Overall Heat Transfer Coefficient and Pressure Drop of a Shell and Tube Heat Exchanger: Experimental Performance Comparison, *International Journal of Thermal Sciences*, *188* (2023), June, 108217
[4] Kim, M., *et al.*, Air-Side Heat Transfer Enhancement in Fin-Tube Heat Exchangers Using Forced Vibrations Under Various Conditions, *International Communications in Heat and Mass Transfer*, *144* (2023), May, 106798
[5] Menni, Y., *et al.*, A Review of Solar Energy Collectors: Models and Applications, *Journal of Applied and Computational Mechanics*, *4* (2018), 4, pp. 375-401
[6] Mohammed Hussein, H. A., *et al.*, Structure Parameters and Designs and Their Impact on Performance of Different Heat Exchangers: A Review, *Renewable and Sustainable Energy Reviews*, *154* (2022), Feb., 111842
[7] Mangrulkar, C. K., *et al.*, Recent Advancement in Heat Transfer and Fluid-flow Characteristics in Cross Flow Heat Exchangers, *Renewable and Sustainable Energy Reviews*, *113* (2019), Oct., 109220
[8] Douadi, O., *et al.*, A Conceptual Framework for Waste Heat Recovery from Compression Ignition Engines: Technologies, Working Fluids & Heat Exchangers, *Energy Conversion and Management: X*, *16* (2022), Dec., 100309
[9] Jafari, S. M., *et al.*, Designing and Application of a Shell and Tube Heat Exchanger for Nanofluid Thermal Processing of liquid Food Products, *Journal of food process engineering*, *41* (2018), 3, 12658

[10] Gil, J. D., *et al.*, A Review from Design to Control of Solar Systems for Supplying Heat in Industrial Process Applications, *Renewable and Sustainable Energy Reviews*, *163* (2022), July, 112461
[11] Habibishandiz, M., Saghir, M. Z., A Critical Review of Heat Transfer Enhancement Methods in the Presence of Porous Media, Nanofluids, and Microorganisms, *Thermal Science and Engineering Progress*, *30* (2022), May, 101267
[12] Menni, Y., *et al.*, Enhancement of Convective Heat Transfer in Smooth Air Channels with Wall-Mounted Obstacles in the Flow Path: A Review, *Journal of Thermal Analysis and Calorimetry*, *135* (2019), Apr., pp. 1951-1976
[13] Menni, Y., *et al.*, Nanofluid Transport in Porous Media: A Review, *Special Topics & Reviews in Porous Media: An International Journal*, *10* (2019), 1, pp. 49-64
[14] Menni, Y., *et al.*, Nanofluid-flow in Complex Geometries – A Review, *Journal of Nanofluids*, *8* (2019), 5, pp. 893-916
[15] Menni, Y., *et al.*, Advances of Nanofluids in Solar Collectors – A Review of Numerical Studies, *Math. Model Eng. Probl.*, *6* (2019), 3, pp. 415-27
[16] Menni, Y., *et al.*, Enhancement of the Turbulent Convective Heat Transfer in Channels Through the Baffling Technique and Oil/Multiwalled Carbon Nanotube Nanofluids, *Numerical Heat Transfer, Part A: Applications*, *79* (2020), 4, pp. 311-351
[17] Menni, Y., *et al.*, Improvement of the Performance of Solar Channels by Using Vortex Generators and Hydrogen Fluid, *Journal of Thermal Analysis and Calorimetry*, *147* (2022), 1, pp. 545-566
[18] Menni, Y., *et al.*, Effects of In-Line Deflectors on the Overall Performance of a Channel Heat Exchanger, *Engineering Applications of Computational Fluid Mechanics*, *15* (2021), 1, pp. 512-529
[19] Menni, Y., *et al.*, Effects of Two-Equation Turbulence Models on the Convective Instability in Finned Channel Heat Exchangers, *Case Studies in Thermal Engineering*, *31* (2022), Mar., 101824
[20] Menni, Y., *et al.*, Baffle Orientation and Geometry Effects on Turbulent Heat Transfer of a Constant Property Incompressible Fluid-flow Inside a Rectangular Channel, *International Journal of Numerical Methods for Heat & Fluid-flow*, *30* (2020), 6, pp. 3027-3052
[21] Demartini, L. C., *et al.*, Numeric and Experimental Analysis of the Turbulent Flow Through a Channel with Baffle Plates, *Journal of the Brazilian Society of Mechanical Sciences and Engineering*, *26* (2004), 2, pp. 153-159
[22] Mahdi, K., *et al.*, Using Obstacle Perforation, Reconfiguration, and Inclination Techniques to Enhance the Dynamic and Thermal Structure of a Top-Entry Channel, *Thermal Science*, *26* (2022), Special Issue 1, pp. S475-S484
[23] Nasiruddin, Siddiqui, M. H., Heat Transfer Augmentation in a Heat Exchanger Tube Using a Baffle, *International Journal of Heat and Fluid-flow*, *28* (2007), 2, pp. 318-328
[24] Launder, B., Spalding, D., The Numerical Computation of Turbulent Flows, *Computer Methods in Applied Mechanics and Energy*, *3* (1974), 2, pp. 269-289
[25] Patankar, S. V., Numerical Heat Transfer and Fluid-flow, McGraw-Hill, New York, USA, 1980
[26] Leonard, B. P., Mokhtari, S., *ULTRA-SHARP Nonoscillatory Convection Schemes for High-Speed Steady Multidimensional Flow*, NASA TM 1-2568, NASA Lewis Research Center: Cleveland, O., USA, 1990

Paper submitted: December 12, 2022
Paper revised: March 21, 2023
Paper accepted: May 24, 2023